Analysis of Compact Silicon Photonic Hybrid Ring External Cavity (SHREC) Wavelength-Tunable Laser Diodes Operating from 1881-1947 nm

Jia Xu Brian Sia, Wanjun Wang, Zhongliang Qiao, Xiang Li, Xin Guo, Jin Zhou, Callum G. Littlejohns, Chongyang Liu, Graham T. Reed, and H. Wang

***Abstract*— The "2 μm waveband", specifically the 1.9 μm wavelength region, is playing an increasingly imperative role in photonics. Development into compact tunable light sources operating at the wavelength region can unlock numerous technological applications. Instances, while not exhaustive, include alleviating the capacity load in fiber communications, H_2O spectroscopy, optical logic, signal processing as well as enabling the optical Kerr effect on silicon. Silicon photonics is a disruptive technology. Through mature silicon processing, recent developments suggest that silicon will emerge as the workhorse of integrated optics. While the realization of a monolithic light source has proved to be challenging, the hybrid/heterogenous Si platforms, consisting of silicon and III-V materials, has stepped to the fore. In this work, we present the study of Vernier-based hybrid silicon photonic wavelength-tunable lasers with an operating range of 1881-1947 nm (66 nm), subject to different coupling gaps (Gap_{mrr}) between the silicon microring resonators (MRRs) and bus waveguide. Wavelength tuning functionality is enabled via the thermo-optic effect of MRRs. Gap_{mrr}, being the smallest feature in the assemble, is highly influential to the characteristics of the SHREC. As such, trends in hybrid laser performance with respect to Gap_{mrr} are measured and analyzed. Slope efficiency, laser output power and side-mode suppression ratio of 0.232 W/A, 28 mW and 42 dB respectively are obtained across the developed lasers. Through the design of the Vernier spectrum and Gap_{mrr}, tuning of laser wavelength from 1881-1947 nm can be achieved by applying only 47.2 mW of thermal power to a single MRR.**

***Index Terms*—Silicon photonics, Si hybrid lasers, tunable lasers, Vernier effect, 2 μm waveband, integrated optics.**

I. Introduction

The immunity of optical interconnection to skin effect and RC time delay has great potential to limit the scope of copper wiring with respect to very-large-scale integration (VLSI) [1]. However, the implementation of photonic integrated circuits (PICs) has not been as pervasive as one would have envisioned. III-V materials constitutes the primary platform of choice for PICs, allowing for the monolithic integration of a wide range optical functions [2], most fundamentally, its highly-efficient light-emission capabilities [3]. Recent developments suggest that the integration of both silicon photonics and III-V may further motivate the development of integrated photonics [4]; fueled by its compatibility with mature CMOS infrastructure, silicon photonic-based PICs can be manufactured at high yield and low cost.

Erbium-doped fiber amplifier (EDFA) [5], low-loss single-mode fiber (SMF) [6], wavelength division multiplexing (WDM) [7] and digital coherent transmission [8] are key components in contemporary telecommunication systems. However, exponentially increasing bandwidth requirements have led to concerns with regards to the upper limit of the SMF [9]. Reports of the thulium-doped fiber amplifier (TDFA) [10]-[12], hollow-core photonic bandgap fiber [13]-[15] and successful demonstration of transmission systems [16]-[18] have highlighted the possibility of the "2 μm waveband" in serving as an adjunct to the present communication infrastructure. Applications of the waveband however extends far beyond fiber-based communications; examples include, while not exhaustive, spectroscopic gas sensing [19], free-space communications [20] and LIDAR [21]. More specifically, the wavelength region centered around 1.9 μm might be decisive in alleviating the load on the O/C-band; HC-PBGF will reach its lowest propagation loss near 1.9 μm [14]-[15], TDFA has also demonstrated to be capable of delivering high small-signal gain at low noise-figure in the wavelength region [10]-[12]. The vicinity of the 1.9 μm wavelength region corresponds to the

This paragraph of the first footnote will contain the date on which you submitted your paper for review. This work is supported in part by the National Research Foundation of Singapore (NRFCRP12-2013-04) and NTU-A*Star Silicon Technologies Centre of Excellence. (*Corresponding author: Hong Wang, Wanjun Wang)* (email: ewanghong@ntu.edu.sg, wang.wangjun@ntu.edu.sg)

J. X. B. Sia, W. Wang, Z. Qiao, X. Li, X. Guo, J. Zhou and H. Wang are with the School of Electrical and Electronic Engineering, Nanyang Technological University, 639798 Singapore (email: jiaxubri001@e.ntu.edu.sg/jxbsia1991@gmail.com)

C. Liu is with Temasek Laboratories@NTU(TL@NTU), Nanyang Technological University, 637553 Singapore.

G. T. Reed and C. G. Littlejohns are with Optoelectronics Research Centre, University of Southampton, Southampton, SO17 1BJ UK.

Z. Qiao is with Key Laboratory of Laser Technology and Optoelectronic Functional Materials of Hainan Province, School of Physics and Electronic Engineering, Hainan Normal University, 571158 China.

absorption window of H_2O [19], [22]-[23] as well as the "prime region" for the implementation of optical logic, signal processing [24] and optical Kerr effect on silicon [25]. In the area of silicon photonics, much of the touted "2 μm waveband" devices are in fact implemented near the 1.9 μm wavelength range [26]-[32]. As such, there is pertinence for further development in the wavelength region.

Silicon photonics has the potential for pervasive technological implications. To date, most fundamental components has been implemented to great effect [26]-[32], [33]-[40], but the realization of the laser source has been more challenging; silicon has an indirect bandgap. Impressive work has been done in Si Raman [41]-[44] and Ge lasers [45], which will potentially lead to the resolution of a high-performance monolithic laser source in the long run. However, in the meanwhile, the high-performance hybrid/heterogenous silicon photonic platform provides an interesting alternative [46]; silicon photonics provides low propagation loss and high integration densities, III-V materials provides high gain values. Prime example includes the demonstration of high power, sub-kHz linewidth lasers [47]-[50].

Up to now, impressive developments have been achieved in hybrid/heterogenous wavelength-tunable lasers operating in the C-band [50]-[56], enabled by the Vernier effect between two microring resonators (MRRs). The reach of this class of lasers is extended above 2 μm in 2016, where the effect of coupling gap between the MRR and bus waveguide (Gap_{mrr}) is studied for the first time [57]. Gap_{mrr}, being the smallest feature in the tunable laser structure, is influential with regards to the characteristic of the SHREC. Thereby, in this work, the effects that Gap_{mrr} will have on laser performance is further studied from [57]. The tunable laser diodes developed in this work operates near the wavelength region of 1.9 μm from 1881-1947 nm (66 nm). Hybrid integration between III-V and silicon photonics is achieved by edge coupling the III-V waveguide to the SHREC (Fig. 1(a)). Such an architecture enables the SHREC and III-V waveguide to be individually optimized, enabling high-power laser emission via strong mode overlap with the gain media [58] and easier thermal management; i.e. III-V waveguide are prone to thermal degradation, locating the III-V component at the edge of the hot VLSI substrate reduces the complexity of thermal management [58]-[59]. Through variations in Gap_{mrr}, changes in slope efficiency (η_s), maximum laser output power, threshold current (I_{th}), phase-shifter efficiency, side-mode suppression ratio (SMSR) and channel uniformity is observed. η_s, maximum laser output power and SMSR as high as 0.232W/A, 28 mW and 42 dB respectively are obtained across the reported tunable lasers. The lowest I_{th} recorded is 356 mA. With only 47.2 mW of power applied on one phase-shifter, the entire discrete tunable range of the laser can be accessed. The scope of the manuscript is as follows. Firstly, theoretical basis and experimental characterization of the wavelength-tunable Vernier filter as a function of Gap_{mrr} is illustrated. Following, the epitaxial structure and the spontaneous emission spectra of the designed semiconductor optical amplifier (SOA) is presented. Lastly, tunable laser performance is analyzed with respect to variations in Gap_{mrr}. The tunable laser with Gap_{mrr} = 180 nm, used for analysis in this work is reported in our previous work [60].

II. SHREC Wavelength Tunable Laser Diode

Fig. 1(a) illustrates the 3-D schematic of the SHREC wavelength-tunable laser diode together with the coordinates that will be standardized in this manuscript. Fig. 1 (b)-(c) shows the micrograph images of the spot-size converter (SSC), wavelength-tunable Vernier cavity and SOA respectively. In order to realize the hybrid laser cavity, a wavelength-tunable Vernier cavity is edged-coupled to the SOA via the Si slab waveguide and the SSC; the SOA provides optical gain, whereas the Vernier cavity enables wavelength-selective feedback. The wavelength-tunable Vernier cavity comprises of two MRRs and an MMI-based reflector; Vernier effect is facilitated by the two MRRs, the MMI-based reflector allows full reflectance. The MMI-based reflector is used due to the fabrication tolerance of the MMI structure [60]. Simulated and

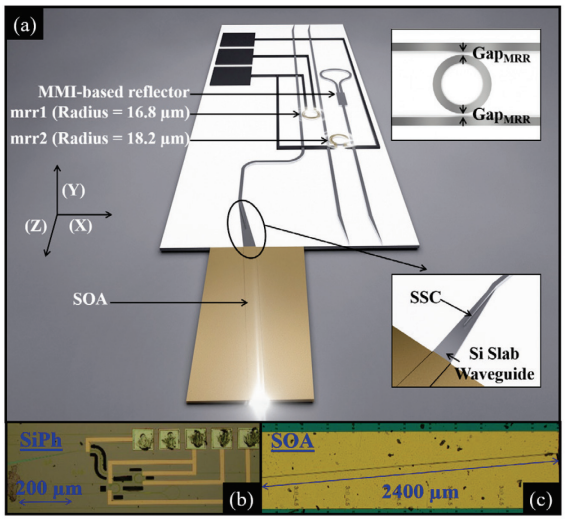

Fig. 1. 3-D schematic of the wavelength-tunable laser diode. Micrograph images of (a) SSC, wavelength-tunable Vernier cavity (c) and SOA.

experimental data of the MMI-based reflector is provided in our previous work [60]; single trip insertion loss of the MMI-based reflector at $\lambda \approx 1947$ nm is 0.538 dB [60]. As indicated in Fig. 1(a), mrr1 and mrr2 has a radius of 16.8 and 18.2 μm respectively. Thermo-optic phase-shifters mounted on top of the MRRs are used to enable thermal control of lasing wavelength. Lasing output occurs at the facet of the SOA as indicated in Fig. 1(a).

The SHREC, consisting of the wavelength-selective Vernier cavity, SSC and Si slab waveguide is fabricated on the 220 nm silicon-on-insulator (SOI) platform via the standard CMOS process. We characterize the propagation loss of the single-mode (TE00) strip waveguide (0.6×0.22 μm^2) to be 3 dB/cm. At the coupling facet of the SHREC to the III-V waveguide, the low-confinement slab (6×0.07 μm^2) waveguide is designed to enable good overlap between both optical modes [60]. A 200 μm-long SSC is used for low-loss conversion from the slab to the strip waveguide that forms the wavelength-selective Vernier cavity [60]. Data with regards to the III-V/silicon coupling

interface as well as the SSC can be found in our previous work [60]. The coupling loss between hybrid integration of the SHREC and SOA is experimentally characterized to be 2.7 dB. This represents the loss from the SOA to the Si slab waveguide, then SSC to the Si strip waveguide. The radii of the MRRs are designed to be 16.8 and 18.2 μm, corresponding to approximate FSRs of 8.9 nm (740 GHz) and 8.5 nm (706 GHz) respectively. After the fabrication of the waveguides, 1.2 μm of SiO_2 cladding is deposited followed by 120 nm of TiN (phase-shifter layer) and 2 μm of Al (routing layer). The footprint of the SHREC is 0.95 × 0.3 mm^2.

A. Wavelength-tunable Vernier filter

We can define the power transmittance spectra at the drop port of a single MRR as (1), where κ is the electric-field coupling coefficient between the bus waveguide and the MRR, θ is the incurred phase of the lightwave after propagating one round in the MRR, α is the waveguide loss coefficient. The theoretical power transmittance spectra of the 2 individual MRRs is presented in Fig. 2 (a).

$$P_{mrr1,\,2} = \left| \frac{-\kappa^{*}\kappa\sqrt{\alpha}\exp(j\sqrt{\theta_{mrr1,\,2}})}{1-(\sqrt{1-|\kappa^{2}|})^{*}(\sqrt{1-|\kappa^{2}|})^{*}\alpha\exp(j\theta_{mrr1,\,2})} \right|^{2} \quad (1)$$

Following, the Vernier spectra can be computed as a product of the power transmittance spectra of the 2 MRRs (2). Fig. 2(b) shows the theoretical Vernier power transmittance spectra.

$$P_{Vernier} = P_{mrr1} \times P_{mrr2} \quad (2)$$

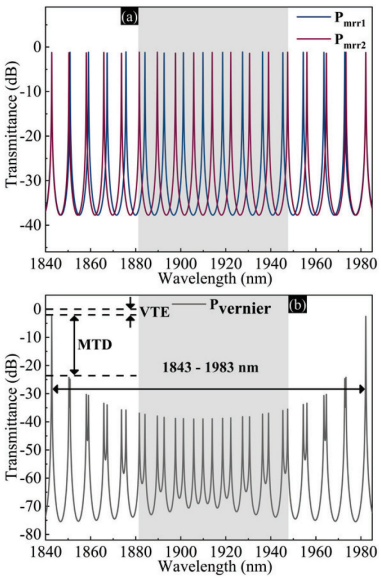

Fig. 2. (a) The red and blue lines indicate the theoretical power transmittance spectra of mrr1 and mrr2 respectively. (b) The grey line indicates the theoretical power transmittance of the Vernier power transmittance spectra; basic definitions of the Vernier power transmittance spectra are indicated. Operation range of the laser is shaded in grey.

By exploiting the thermo-optic effect of silicon through the phase-shifters, one will be able to control the wavelength corresponding to the lowest loss in the laser cavity via the overlap of the 2 MRR resonant peaks; single and dual shifter tuning will facilitate discrete and fine tuning of laser wavelength respectively. Consequently, the cavity longitudinal mode closest to the Vernier transmittance peak will be the lasing wavelength. Modal transmittance difference (MTD) as indicated in Fig. 2(b), is the extent of transmittance difference between the main and adjacent peaks. It is the primary feature that determines the extent of mode-selectivity with regards to the SHREC, enabling lasing of the specific cavity longitudinal mode nearest to the Vernier peak via mode competition. Vernier transmittance efficiency (VTE) indicates the insertion loss at the wavelength of the Vernier peak (Fig. 2(b)). In this work, the designed Vernier filter has an FSR of 140 nm (1843-1983 nm). The demonstrated tuning bandwidth (1881-1947 nm) of the laser reported in this work is shaded in grey at Fig. 2(a)-(b).

Fig. 3(a)-(f) shows the normalized measured and theoretical Vernier power transmittance spectra with respect to Gap_{mrr} = 160, 180, 200, 220, 240, 260 nm; experimental data are shown to resemble theoretical expectations closely. The lower-half of each individual plot corresponds the case when the power supplied to phase-shifter 1 and 2 (H_{mrr1}, H_{mrr2}) are 0 mW. The upper-half of Fig. 3(a)-(f) illustrates the resultant spectra when H_{mrr2} = 0 mW and H_{mrr1} = 15.5, 12.4, 11.1, 10.0, 8.7, 7.8 mW are applied respectively; a larger Gap_{mrr} would lead to an increased MRR Q-factor, as such, the effective MRR optical length will increase, leading to gains in phase-shifter efficiency. Due to the detection limit of the detector (Artifex, OPM500), we are not able to characterize all the features of the Vernier spectra. We measured the Vernier filter from 1935-1985 nm due to the maximum tunable range of our tunable laser light source (Thorlabs, customized). The wavelength sweep resolution is 5 pm. Through the appropriate application of H_{mrr1}, we are be able to red-shift the resonant wavelength of mrr1 by approximately 2 nm from H_{mrr1} = 0 mW (Fig, 3(a)-(f), lower-half), resulting in a Vernier transmittance peak at λ ≈ 1947 nm (Fig. 3(a)-(f), upper-half). This corresponds to the longest demonstrated wavelength of the tunable laser in this work.

As reference, the theoretical value of κ as a function of Gap_{mrr} (140-320 nm) is presented (Fig. 4(a)). The characteristics of the Vernier filter is summarized experimentally and theoretically in Fig. 4(b)-(e). It can be seen that there is a close match between experimental data and theoretical trends. According to Fig. 4(b), when Gap_{mrr} is increased, MTD rises. VTE however, drops when Gap_{mrr} is increased (Fig. 4(c)); laser cavity loss is expected to increase. Another important point of consideration is the full-width half maximum (FWHM) and Q-factor of the individual MRRs. FWHM decreases and Q-factor increases when Gap_{mrr} becomes larger (Fig. 4(d)-(e)). MRRs with low FWHM has a greater propensity to be misaligned by environmental thermal drifts. Furthermore, as indicated in the previous paragraph, while a higher Q-factor will lead to higher phase-shifter efficiency, it can also result in greater sensitivity to inconsistencies in environment temperature [61]-[62]. The data presented suggests that the implications of Gap_{mrr} on the Vernier filter is critical for subsequent Vernier-based laser design.

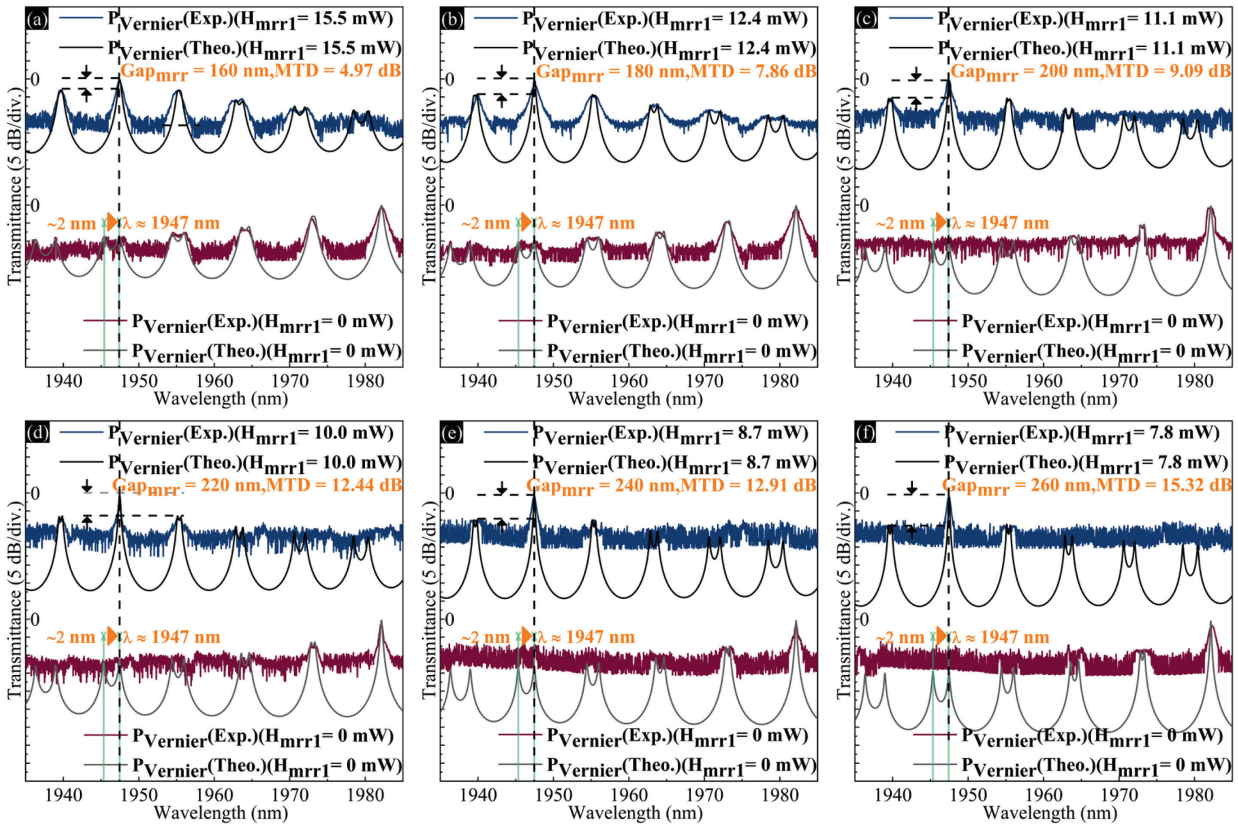

Fig. 3. Measured and theoretical Vernier power transmittance when $H_{mrr1} = H_{mrr2} = 0$ mW (lower half) (a) $Gap_{mrr} = 160$ nm, $H_{mrr1} = 15.5$ mW, $H_{mrr2} = 0$ mW (upper half), (b) $Gap_{mrr} = 180$ nm, $H_{mrr1} = 12.4$ mW, $H_{mrr2} = 0$ mW (upper half), (c) $Gap_{mrr} = 200$ nm, $H_{mrr1} = 11.1$ mW, $H_{mrr2} = 0$ mW (upper half), (d) $Gap_{mrr} = 220$ nm, $H_{mrr1} = 10.0$ mW, $H_{mrr2} = 0$ mW (upper half), (e) $Gap_{mrr} = 240$ nm, $H_{mrr1} = 8.7$ mW, $H_{mrr2} = 0$ mW (upper half), (f) $Gap_{mrr} = 260$ nm, $H_{mrr1} = 7.8$ mW, $H_{mrr2} = 0$ mW (upper half).

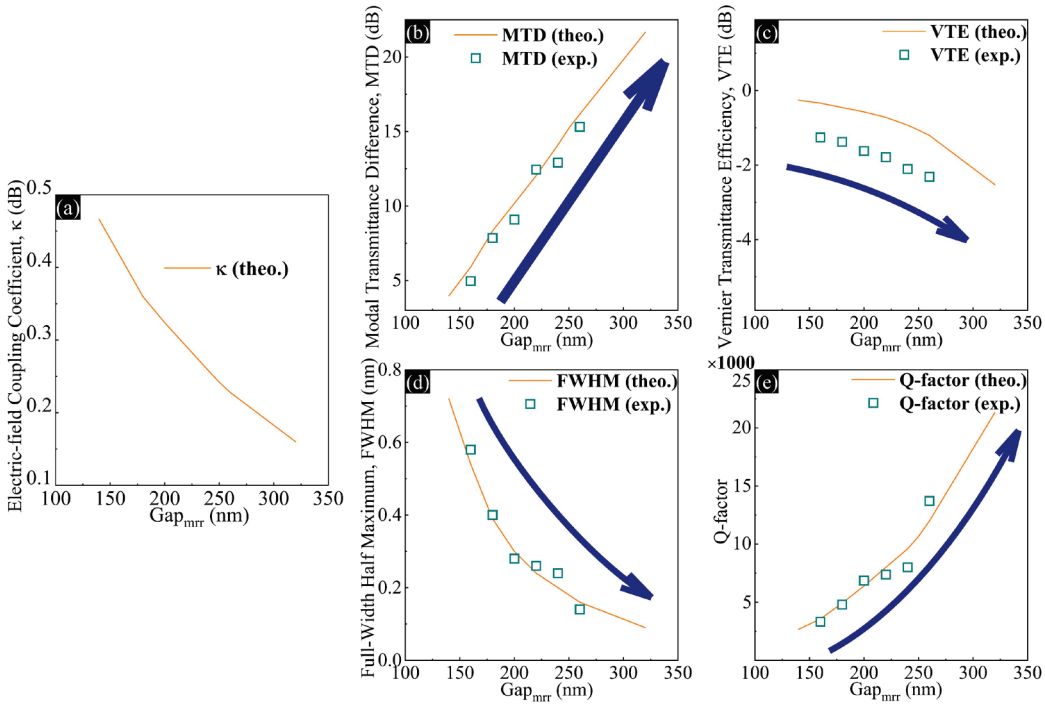

Fig. 4. (a) Theoretical κ as a function of Gap_{mrr} = 140-320 nm. (b) Theoretical MTD as a function of Gap_{mrr} = 140-320 nm, experimental MTD when Gap_{mrr} = 160, 180, 200, 220, 240, 260 nm. (c) Theoretical VTE as a function of Gap_{mrr} = 140-320 nm, experimental VTE when Gap_{mrr} = 160, 180, 200, 220, 240, 260 nm. (d) Theoretical MRR FWHM as a function of Gap_{mrr} = 140-320 nm, experimental MRR FWHM when Gap_{mrr} = 160, 180, 200, 220, 240, 260 nm. (e) Theoretical MRR Q-factor as a function of Gap_{mrr} = 140-320 nm, experimental MRR Q-factor when Gap_{mrr} = 160, 180, 200, 220, 240, 260 nm.

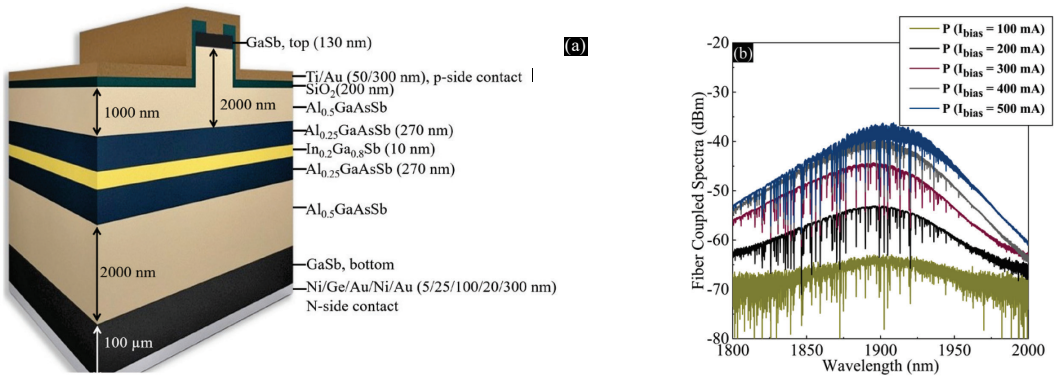

Fig. 5. (a) Cross-sectional depiction of the InGaSb/AlGaAsSb SOA. (b) Measured spontaneous emission spectra of the InGaSb/AlGaAsSb SOA when I_{bias} = 100, 200, 300, 400, 500 mA.

B. *InGaSb/AlGaAsSb SOA*

In this work, the designed epitaxial structure intended for the fabrication of the SOA was grown on a (100) n-GaSb substrate using the molecular beam epitaxy (MBE); cross-section (x-y plane) of the epitaxial structure is illustrated in Fig. 5(a). The designed structure is composed of a 10 nm-thick $In_{0.2}Ga_{0.8}Sb$ single quantum well (SQW) sandwiched by 270 nm-thick $Al_{0.25}GaAsSb$ barrier layers. The cladding comprises of 2000 nm-thick $Al_{0.5}GaAsSb$ layers. The barrier and cladding layers, with exception to the SQW layer, are latticed matched to the GaSb substrate; 1.26 % compressive strain is exerted on the SQW layer.

The fabrication process steps of the SOA are similar to our previous work [63]. Firstly, the ridge (6.4 × 1.0 µm^2) was defined using UV lithography and wet chemical etching. After which, SiO_2 was deposited using the plasma-enhanced chemical vapor deposition (PECVD) for injection current confinement. Following, we defined a contact window at the center of the ridge using UV lithography and buffered oxide etch (BOE) process. Chemical-mechanical process (CMP) was carried out on the GaSb to reduce the thickness of the SOA; the resultant thickness is approximately 100 µm. A thinner SOA cross-section will facilitate cleaving, reduce series resistance, as well as allowing responsive thermal control during laser operation. Ti/Au and Ni/Ge/Au/Ni/Au are deposited using electron-beam evaporation to form the p and n side ohmic contacts respectively. Finally, the III-V waveguide is cleaved to be 2.4 mm-long and bonded onto a heat sink. Due to the fact that Fabry-Perot (F-P) oscillations can reduce the single-mode stability of the tunable laser [53], the III-V waveguide is angled at 4.5°. The epitaxial structure of the SOA is designed to operate about 1.9 µm wavelength region. By measuring the output at the facet of the waveguide, the spontaneous emission spectra at I_{bias} = 100, 200, 300, 400, 500 mA is presented in Fig. 5(b); the emission spectra resembles that obtained from our previous work [64], implying that reflections within the III-V has been successfully subdued.

III. Experimental Characterization and Analysis

According to Snell's law, the Si slab waveguide is angled at 9.8° to in accordant to the slant-angle of the III-V waveguide. The facet quality of the Si slab waveguide was improved via polishing to reduce edge-coupling losses. Integration of the hybrid laser cavity was carried out by placing the SHREC and SOA on 2 different x/y/z precision alignment stages. Two separate thermoelectric controllers (Arroyo Instruments, 5305 TECSource) are connected to each stage for thermal management. The laser output is coupled directly into the opening of the photodetector (Thorlabs, S148C) or coupled via a lensed-fiber, connected to optical spectrum analyzer (Yokogawa, AQ6375) for power or spectra characterization respectively. The coupling loss between laser output facet and lensed fiber is 10 dB during spectra characterization. For power characterization, as all laser emission is coupled into the opening of the photodetector which integrates the sum of the power under the lasing spectra, coupling loss of laser power off-chip is negligible in our setup.

Fig. 6(a)-(d) are obtained when λ ≈ 1921 nm. The L-I curves of the tunable laser up to I_{th} = 470 mA when Gap_{mrr} = 140, 180, 250, 320 nm are illustrated in Fig. 6(a); values for η_s are indicated at Fig. 6(b).

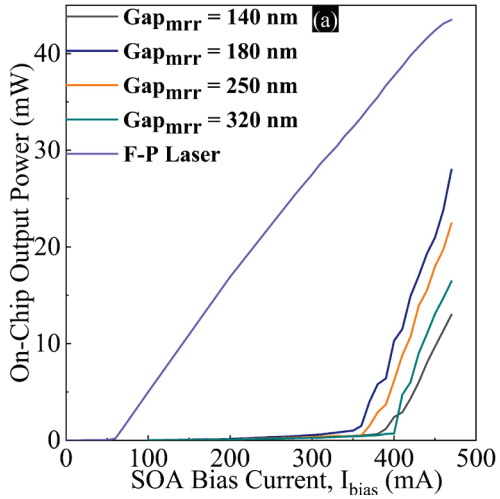

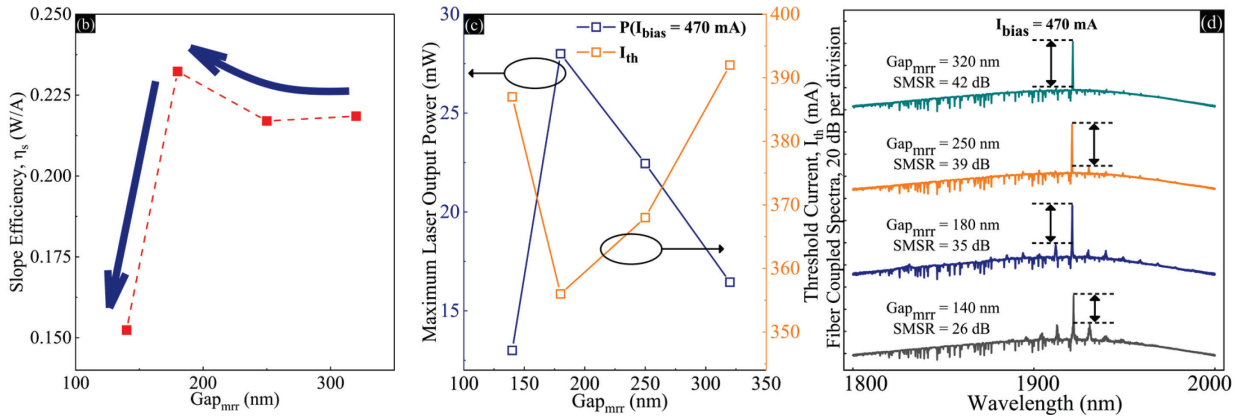

Fig. 6. (a) Laser output power against I_{bias} for Gap_{mrr} = 140, 180, 250, 320 nm and F-P laser. (b) η_s for Gap_{mrr} = 140, 180, 250, 320 nm. (c) Maximum demonstrated laser output power and I_{th} for Gap_{mrr} = 140, 180, 250, 320 nm. (d) Fiber coupled spectra corresponding to Gap_{mrr} = 140, 180, 250, 320 nm when I_{bias} = 470 mA.

Room temperature continuous-wave operation is achieved for all cases. The losses of the SHREC in the laser cavity is the summation of III-V/Si coupling loss [60], SSC, VTE and MMI-based reflector insertion losses [60]. The round-trip insertion loss (L_{SHREC}) of the silicon wavelength tunable cavity can be defined by the following (3).

$$L_{SHREC} = 2(L_{VTE} + L_{MMI} + L_{SSC} + L_{SOA/Si}) \quad (3)$$

The simulated insertion loss values of the MMI (L_{MMI}), SSC (L_{SSC}) and SOA/Si coupling loss ($L_{SOA/Si}$) are 0.274 ($\lambda \approx 1947$ nm), 0.986 and 1.46 dB respectively [60]. L_{VTE} can be found in Fig. 4 (c). As a reference at $\lambda \approx 1947$ nm, the simulated L_{SHREC} for laser diodes presented in Fig. 6(a) are shown in Tab.1. Due to high L_{SHREC}, it can be seen from Fig. 6(a) that the I_{th} of the hybrid laser diodes is significantly larger, in comparison to a solitary F-P laser.

TABLE I
SIMULATED L_{SHREC} FOR LASER DIODES PRESENTED IN FIG. 6(A)

Gap_{mrr} (nm)	L_{SHREC} (dB)
140	5.956
180	6.35
250	7.564
320	10.498

The VTE, is presented in Fig. 4(c); increasing Gap_{mrr} would result in a reduction of VTE and vice versa. It can be seen that as Gap_{mrr} decreases from 320 nm to 140 nm, η_s reaches a peak value of 0.232 W/A at Gap_{mrr} = 180 nm, before dropping drastically to 0.152 W/A at Gap_{mrr} = 140 nm. A similar trend is observed with regards to maximum demonstrated laser output power in Fig. 6(c); maximum laser output power reaches a maximum at 28 mW when Gap_{mrr} = 180 nm, minimum of 13 mW when Gap_{mrr}= 140 nm. The inverse trend to η_s and maximum laser output power is observed with regards to I_{th} in Fig. 6(c); I_{th} decreases with Gap_{mrr} and reaches a minimum value of 356 mA at Gap_{mrr} = 180 nm before increasing again at Gap_{mrr} = 140 nm. Fig. 6(a)-(c) point to Gap_{mrr} = 180 nm being the optimal value with regards to η_s, maximum laser output power and I_{th}. At I_{bias} = 470 mA, single-mode lasing with side-mode suppression ratio of 26, 35, 39, 42 dB corresponding to Gap_{mrr} = 140, 180, 250, 320 nm respectively was obtained (Fig. 6(d)).

The improvement of η_s, maximum laser output power and I_{th} when Gap_{mrr} decreases from 320 to 180 nm can be attributed to the reduced laser cavity losses brought about by a decrease in VTE (Fig. 4(c)). However, Gap_{mrr} = 140 nm bucks the trend in all the above-mentioned laser performance metrics. According to Fig. 6(d) when Gap_{mrr} reduces from 180 to 140 nm, there is a large drop in SMSR from 35 to 26 dB. Significantly increased amplified spontaneous emission (ASE) due to low MTD is the reason behind the phenomena; the roll-off value of MTD occurs when Gap_{mrr} = 140 nm, is predicted to be 3.97 dB theoretically (Fig. 4(b)). When Gap_{mrr} is small (Gap_{mrr} = 140 nm), the reflectance difference between the wavelength corresponding to the Vernier peaks and the rest of the spectrum will be low, as a result of a low MTD (Fig. 4(b)). Consequently, unwanted reflections at the secondary peaks of the Vernier spectrum is more significant in the laser cavity leading to the significant onset of ASE. This effect can be seen from the relative strength of ASE when Gap_{mrr} = 140 nm in comparison to larger Gap_{mrr} (Fig. 6(d), 7(a)-(d)). ASE is incoherent and limits the maximum gain in the SOA [65]. Thereby, attributing to the degradation in η_s, maximum laser output power and I_{th}. Lasing performance in terms of η_s, maximum output power and I_{th} are determined by the interplay between the MTD and VTE of the SHREC.

Fig. 7(a)-(d) shows the superimposed lasing spectra pertaining to lasers with Gap_{mrr} = 140, 180, 250, 320 nm respectively when I_{bias} = 450 mA. Tuning range of 1881-1947 nm (66 nm) are achieved. We are unable to state definitively, the limiting factor in regard to the tunable range of the laser diodes. As confirmed in Fig. 6(d), 7(a)-(d), increases in Gap_{mrr} will lead to clear improvement in SMSR due to larger MTD (Fig. 4(b)); strength and number of parasitic oscillations are significantly reduced, indicating lower ASE. Through the increase of H_{mrr1}, the resonant peaks of mrr1 will red-shift, subsequently, the Vernier transmittance peak will blue-shift in step sizes corresponding to FSR_{mrr2} via the overlap of the 2 resonant peaks (Fig. 2(a)-(b)), lasing will occur at the

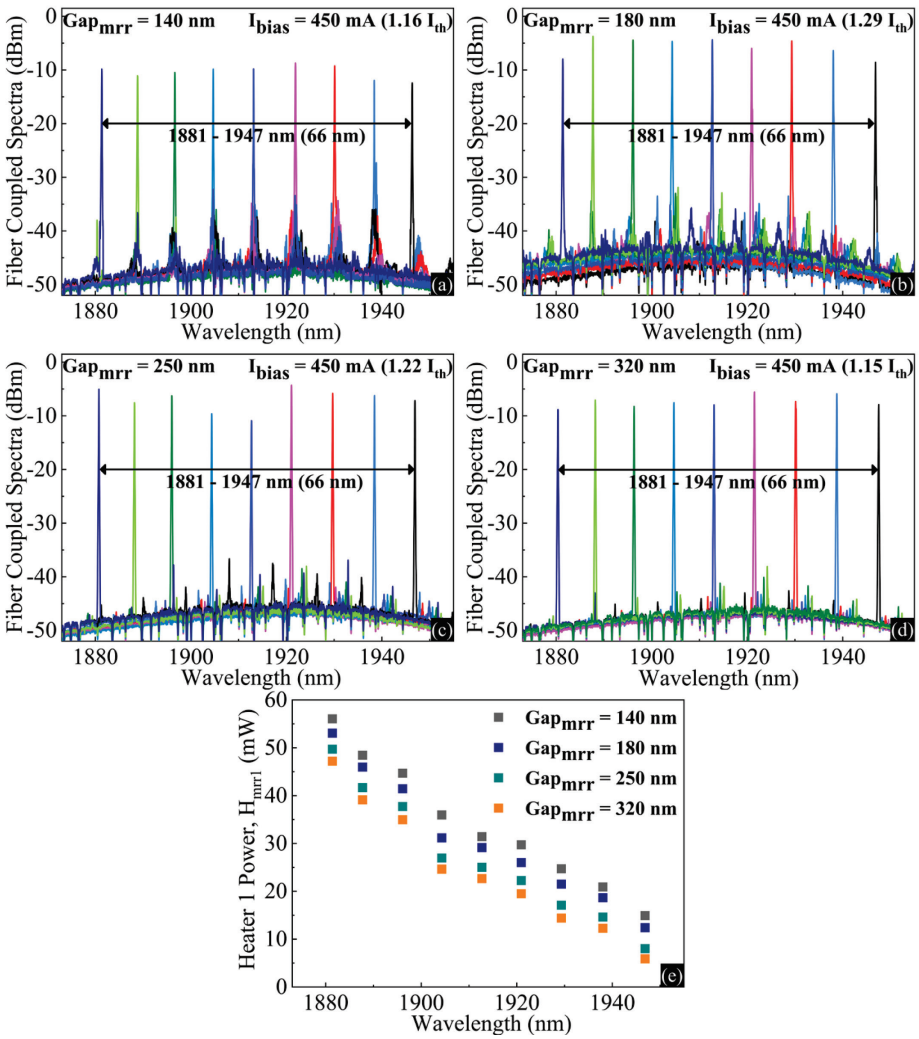

Fig. 7. Superimposed fiber coupled spectra of tunable lasers with different Gap$_{mrr}$s (a) Gap$_{mrr}$ = 140 nm, (b) Gap$_{mrr}$ = 180 nm, (c) Gap$_{mrr}$ = 250 nm, (d) Gap$_{mrr}$ = 320 nm. (e) H$_{mrr1}$ corresponding to each discrete wavelength within the tuning range of the lasers (Gap$_{mrr}$ = 140, 180, 250, 320 nm).

longitudinal mode that experience the least cavity loss through mode competition. The values of H$_{mrr1}$ corresponding to each demonstrated lasing wavelength of the laser diodes (Fig. 7(a)-(d)) are illustrated in Fig. 7(e). Although only H$_{mrr1}$ is utilized in this work, tuning of H$_{mrr2}$ can also achieve discrete tuning. The only exception is that lasing wavelength will shift towards longer wavelength in steps of FSR$_{mrr1}$ in regard to increment in H$_{mrr2}$. Fig. 7 (e) illustrates an increase in phase-shifter efficiency when Gap$_{mrr}$ is increased, this is in line with the trend for H$_{mrr1}$ values observed in Fig. 3(a)-(f). As mentioned earlier, the increase in phase-shifter efficiency can be attributed to longer effective optical length of the MRR due to larger Gap$_{mrr}$ (higher Q-factor) [51]. With H$_{mrr}$ as low as 47.2 mW, discrete tuning of lasing wavelength from 1881-1947 can be obtained.

SMSR implies the amount of power that is generated in the main longitudinal mode. High SMSR is required for a wide range of applications such as high-end optical communications and spectroscopic sensing. In addition, high channel uniformity (extent of variability of SMSR) across the lasing channels is desirable. Low channel uniformity can introduce noise into measurement/detection, potentially impacting system

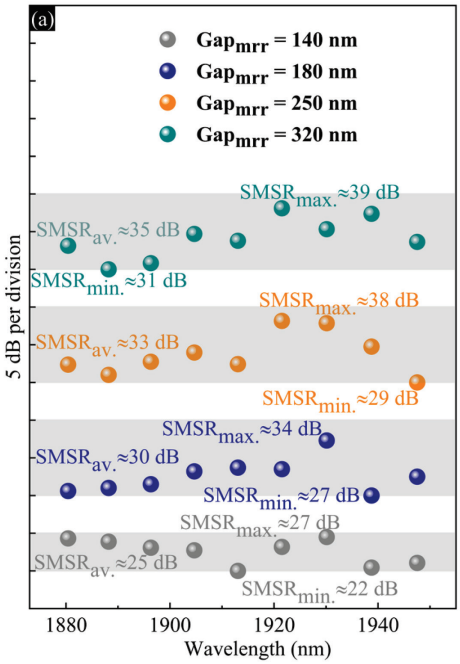

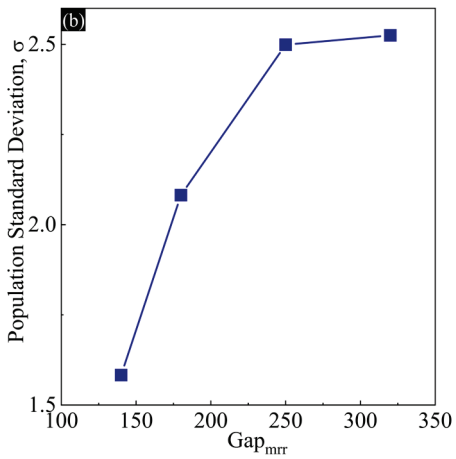

Fig. 8. (a) Distribution of SMSR at each demonstrated discrete lasing wavelength when Gap_{mrr} = 140, 180, 250, 320 nm; values of $SMSR_{min.}$, $SMSR_{max.}$ and $SMSR_{av.}$ indicated according to the color of the scatter plots. (b) σ of SMSR when Gap_{mrr} = 140, 180, 250, 320 nm.

performance [66]-[67]. Fig. 8(a) illustrates the distribution of SMSR across the discrete tuning wavelengths obtained from Fig. 7(a)-(d). While larger Gap_{mrr} can result in a higher SMSR (minimum ($SMSR_{min.}$), maximum ($SMSR_{max.}$) average ($SMSR_{av.}$)), channel uniformity decreases. In Fig. 8(b), we show population standard deviation (σ) of the SMSR as a function of Gap_{mrr}. Increases in σ as a result of larger Gap_{mrr} can be attributed to the increased tendency for MRR resonant peaks with lower FWHM (Fig. 4(d)) and higher Q-factor (Fig. 4(e)) to be misaligned by environmental thermal drifts [61]-[62], impacting wavelength-stability of the wavelength tunable cavity.

IV. Discussion

In response to the potential of the 1.9 µm wavelength region in enabling a wealth of applications, we developed the SHREC wavelength-tunable lasers with an operating range of 1881-1947 nm (66 nm). This is made possible through the integration of appropriately designed SHREC and SOA chips. η_s, maximum laser output power and SMSR up to 0.232 W/A, 28 mW and 42 dB respectively are achieved across the developed laser diodes. Via the increase in MRR Q-factor through Gap_{mrr}, higher phase-shifter efficiency can be obtained. The Vernier transmittance spectra of the SHREC is highly sensitive to Gap_{mrr}, the smallest feature of the laser. By changing Gap_{mrr}, trends in laser performance metrics are studied and analyzed. The findings of this manuscript can be summarized as follows:

1) Optimal η_s, maximum laser output power and I_{th} can be achieved when Gap_{mrr} = 180 nm. Increasing Gap_{mrr} beyond 180 nm will lead to degradation of these parameters due to decreased VTE (Fig. 4(c)); laser cavity loss is increased. Decreasing Gap_{mrr} from 180 nm to the roll-off value 140 nm will also diminish laser performance. The drop in the mentioned laser performance metrics is due to significant onset of ASE brought about by the low MTD of the Vernier spectra ($MTD_{estimated}$ = 3.97 dB).

2) Phase-shifter efficiency increases as Gap_{mrr} becomes larger; increasing Gap_{mrr} will result in a higher MRR Q-factor, resulting in a longer effective MRR length.

3) SMSR rises with increasing Gap_{mrr}. A high MTD resulting from a large Gap_{mrr} will enhance the wavelength-selectivity of the SHREC (Fig. 4(b)).

4) Channel uniformity decreases with increments in Gap_{mrr}. Larger Gap_{mrr} will serve to reduce the FWHM and increase the Q-factor of the 2 MRR resonant peaks, increasing the propensity to be misaligned by environmental thermal fluctuations [61]-[62].

V. Conclusion

In this work, we demonstrate SHREC wavelength tunable laser diodes, subjected to a range of Gap_{mrr}, operating from 1881-1947 nm. We conclude that influence of Gap_{mrr} on laser performance is multi-faceted, under the condition that the roll-off value of Gap_{mrr} is not violated (i.e. Gap_{mrr} = 140 nm), improving a specific performance index will lead to the degradation of another. Laser design should therefore be aimed at optimizing the value of Gap_{mrr} to fulfil the performance requirement of the targeted application (i.e. high SMSR or high output power). Besides the demonstration of high-performance SHREC wavelength-tunable laser diodes operating near the 1.9 µm wavelength region (1881-1947 nm), the proceedings of this work aim to provide useful data and trends in enabling future Vernier-based laser design.

Acknowledgement

This work is supported in part by the National Research Foundation of Singapore (NRFCRP12-2013-04) and NTU-A*Star Silicon Technologies Centre of Excellence.

References

[1] S. Arai, N. Nishiyama, T. Maruyama, and T. Okumura, "GaInAsP/InP Membrane Lasers for Optical Interconnects," *IEEE J. Sel. Top. Quantum Electron.*, vol. 17, no. 5, pp. 1381–1389, 2011.

[2] H. Zhao, S. Pinna, F. Sang, B. Song, S. T. S. Brunelli, L. A. Coldren, and J. Klamkin, "High-Power Indium Phosphide Photonic Integrated Circuits," *IEEE J. Sel. Top. Quantum Electron.*, vol. 25, no. 6, p. 4500410, 2019.

[3] P. Doussiere, "Laser integration on silicon," *IEEE 14th International Conference on Group IV Photonics (GFP)*, 2017.

[4] D. Thomson, A. Zilkie, J. E. Bowers, T. Komljenovic, G. T. Reed, L. Vivien, D. Marris-Morini, E. Cassan, L. Virot, J. Fédéli, J. Hartman, J. H. Schmid, D. Xu, F. Boeuf, P. O'Brien, G. Z. Mashanovich, and M. Nedeljkovic, "Roadmap on silicon photonics," *J. Optics-UK*, vol. 18, no. 7, p. 073003, 2016.

[5] E. Desurvire, *Erbium-doped fiber amplifiers: principles and applications.* New York, NY: Wiley-Interscience, 2002.

[6] K. Nagayama, M. Kakui, M. Matsui, T. Saitoh, and Y. Chigusa, "Ultra-low-loss (0.1484 dB/km) pure silica core fibre and extension of transmission distance," *Electron. Lett.*, vol. 38, no. 20, pp. 1168–1169, 2002.

[7] C. Brackett, "Dense wavelength division multiplexing networks: principles and applications," *IEEE J. on Sel. Areas Commun.*, vol. 8, no. 6, pp. 948–964, 1990.

[8] S. J. Savory, "Digital Coherent Optical Receivers: Algorithms and Subsystems," *IEEE J. of Sel. Top. in Quantum Electron.*, vol. 16, no. 5, pp. 1164–1179, 2010.

[9] D. J. Richardson, "Filling the Light Pipe," *Science*, vol. 330, no. 6002, pp. 327–328, 2010.
[10] Z. Li, Y. Jung, J. M. O. Daniel, N. Simakov, M. Tokurakawa, P. C. Shardlow, D. Jain, J. K. Sahu, A. M. Heidt, W. A. Clarkson, S. U. Alam, and D. J. Richardson, "Exploiting the short wavelength gain of silica-based thulium-doped fiber amplifiers," *Opt. Lett.*, vol. 41, no. 10, pp. 2197–2200, 2016.
[11] Z. Li, A. M. Heidt, N. Simakov, Y. Jung, J. M. O. Daniel, S. U. Alam, and D. J. Richardson, "Diode-pumped wideband thulium-doped fiber amplifiers for optical communications in the 1800 – 2050 nm window," *Opt. Express*, vol. 21, no. 22, pp. 26450–26455, 2013.
[12] J. Wang, S. Liang, Y. Jung, Q. Kang, S.-U. Alam, and D. J. Richardson, "Broadband Silica-Based Thulium Doped Fiber Amplifier Employing Dual-Wavelength Pumping," *Conference on Lasers and Electro-Optics (CLEO)*, 2016.
[13] F. Poletti, N. V. Wheeler, M. N. Petrovich, N. Baddela, E. N. Fokoua, J. R. Hayes, D. R. Gray, Z. Li, R. Slavík, and D. J. Richardson, "Towards high-capacity fibre-optic communications at the speed of light in vacuum," *Nat. Photonics*, vol. 7, no. 4, pp. 279–284, 2013.
[14] P. J. Roberts, F. Couny, H. Sabert, B. J. Mangan, D. P. Williams, L. Farr, M. W. Mason, A. Tomlinson, T. A. Birks, J. C. Knight, and P. S. J. Russell, "Ultimate low loss of hollow-core photonic crystal fibres," *Opt. Express*, vol. 13, no. 1, pp. 236–244, 2005.
[15] B. J. Mangan, L. Farr, A. Langford, P. J. Roberts, D. P. Williams, F. Couny, M. Lawman, M. Mason, S. Coupland, R. Flea, H. Sabert, T. A. Birks, J. C. Knight, and P. St. J. Russel, "Low loss (1.7 dB/km) hollow core photonic bandgap fiber," *Optical Fiber Communication (OFC 2004)*, 2004.
[16] M. N. Petrovich, F. Poletti, J. P. Wooler, A. Heidt, N. Baddela, Z. Li, D. Gray, R. Slavík, F. Parmigiani, N. Wheeler, J. Hayes, E. Numkam, L. Grűner-Nielsen, B. Pálsdóttir, R. Phelan, B. Kelly, J. O'Carroll, M. Becker, N. Macsuibhne, J. Zhao, F. G. Gunning, A. Ellis, P. Petropoulos, S. Alam, and D. Richardson, "Demonstration of amplified data transmission at 2 μm in a low-loss wide bandwidth hollow core photonic bandgap fiber," *Opt. Express*, vol. 21, no. 23, pp. 28559–28569, 2013.
[17] H. Zhang, N. Kavanagh, Z. Li, J. Zhao, N. Ye, Y. Chen, N. V. Wheeler, J. P. Wooler, J. R. Hayes, S. R. Sandoghchi, F. Poletti, M. N. Petrovich, S. U. Alam, R. Phelan, J. O'Carroll, B. Kelly, L. Grüner-Nielsen, D. J. Richardson, B. Corbett, and F. C. G. Gunning, "100 Gbit/s WDM transmission at 2 μm: transmission studies in both low-loss hollow core photonic bandgap fiber and solid core fiber," *Opt. Express*, vol. 23, no. 4, pp. 4946–4951, 2015.
[18] H. Zhang, M. Gleeson, N. Ye, N. Pavarelli, X. Ouyang, J. Zhao, N. Kavanagh, C. Robert, H. Yang, P. E. Morrissey, K. Thomas, A. Gocalinska, Y. Chen, T. Bradley, J. P. Wooler, J. R. Hayes, E. N. Fokoua, Z. Li, S. U. Alam, F. Poletti, M. N. Petrovich, D. J. Richardson, B. Kelly, J. O'Carroll, R. Phelan, E. Pelucchi, P. O'Brien, F. Peters, B. Corbett, and F. Gunning, "Dense WDM transmission at 2 μm enabled by an arrayed waveguide grating," *Opt. Lett.*, vol. 40, no. 14, pp. 3308-3311, 2015.
[19] T. Milde, C. Assmann, A. Jimenez, M. Honsberg, J. O'Gorman, W. Schade, and J. Sacher, "Single mode GaSb diode lasers for sensor applications in a long wavelength regime," *Appl. Opt.*, vol. 56, no. 31, pp. H45–H50, 2017.
[20] K. Scholle, S. Lamrini, P. Koopmann, and P. Fuhrberg, "2 μm Laser Sources and Their Possible Applications," *Frontiers in Guided Wave Optics and Optoelectronics*, 2010.
[21] T. M. Taczak, and D. K. Killinger, "Development of a tunable, narrow-linewidth, cw 2066-μm Ho:YLF laser for remote sensing of atmospheric CO_2 and H_2O," *Appl. Opt.*, vol. 37, no. 36, pp. 8460–8476, 1998.
[22] R. M. Sullenberger, S. Kaushik, and C. M. Wynn, "Photoacoustic communications: delivering audible signals via absorption of light by atmospheric H_2O," *Opt. Lett.*, vol. 44, no. 3, pp. 622–625, 2019.
[23] M. Melieres, and C. Marechal, "The impact of the atmosphere on radiation," in *Climate Change: Past, Present and Future*, Wiley Blackwell, 2015, ch. 7, pp. 61-69.
[24] F. Gunning, and B. Corbett, "Time to Open the 2-μm Window?" *Opt. Photonics News*, vol. 30, no. 3, pp. 42-47, 2019.
[25] A. D. Bristow, N. Rotenberg, and H. M. V. Driel, "Two-photon absorption and Kerr coefficients of silicon for 850–2200nm," *Appl. Phys. Lett.*, vol. 90, no. 19, p. 191104, 2007.
[26] D. Liu, H. Wu, and D. Dai, "Silicon Multimode Waveguide Grating Filter at 2 μm," *J. Lightwave Technol.*, vol. 37, no. 10, pp. 2217–2222, 2019.
[27] Y. Yin, R. Cao, J. Guo, C. Liu, J. Li, X. Feng, H. Wang, W. Du, A. Qadir, H. Zhang, Y. Ma, S. Gao, Y. Xu, Y. Shi, L. Tong, and D. Dai, "High-Speed and High-Responsivity Hybrid Silicon/Black-Phosphorus Waveguide Photodetectors at 2 μm," *Laser Photonics Rev.*, p. 1900032, 2019.
[28] W. Cao, D. Hagan, D. J. Thomson, M. Nedeljkovic, C. G. Littlejohns, A. Knights, S. Alam, J. Wang, F. Gardes, W. Zhang, S. Liu, K. Li, M. S. Rouifed, G. Xin, W. Wang, H. Wang, G. T. Reed, and G. Z. Mashanovich, "High-speed silicon modulators for the 2 μm band," *Optica*, vol. 5, no. 9, pp. 1055-1062, 2018.
[29] J. J. Ackert, D. J. Thomson, L. Shen, A. C. Peacock, P. E. Jessop, G. T. Reed, G. Z. Mashanovich, and A. P. Knights, "High-speed detection at two micrometres with monolithic silicon photodiodes," *Nat. Photonics*, vol. 9, no. 6, pp. 393–396, 2015.
[30] J. Li, Y. Liu, Y. Meng, K. Xu, J. Du, F. Wang, Z. He, and Q. Song, "2-μm Wavelength Grating Coupler, Bent Waveguide, and Tunable Microring on Silicon Photonic MPW," *IEEE Photonics Tech. Lett.*, vol. 30, no. 5, pp. 471–474, 2018.
[31] D. Hagan, M. Ye, P. Wang, J. C. Cartledge, and A. P. Knights, "High-speed performance of a TDFA-band micro-ring resonator modulator and detector," *Opt. Express*, vol. 28, no. 11, pp. 16845-16856, 2020.
[32] J. X. B. Sia, X. Li, Z. Qiao, X. Guo, J. Zhou, C. G. Littlejohns, C. Liu, G. T. Reed, W. Wang, and H. Wang, "1 × N (N = 2, 8) Silicon Selector Switch for Prospective Technologies at the 2 μm Waveband," *IEEE Photonics Technol. Lett.*, vol. 32, no. 18, pp. 1127-1130, 2020.
[33] J. Sun, R. Kumar, M. Sakib, J. B. Driscoll, H. Jayatilleka, and H. Rong, "A 128 Gb/s PAM4 Silicon Microring Modulator With Integrated Thermo-Optic Resonance Tuning," *J. Lightwave Technol.*, vol. 37, no. 1, pp. 110-115, 2019.
[34] X. Wang, W. Shi, H. Yun, S. Grist, N. A. F. Jaeger, and L. Chrostowski, "Narrow-band waveguide Bragg gratings on SOI wafers with CMOS-compatible fabrication process," *Opt. Express*, vol. 20, no. 14, pp. 15547–15558, 2012.
[35] Y. Jiang, W. Jiang, L. Gu, X. Chen, and R. T. Chen, "80-micron interaction length silicon photonic crystal waveguide modulator," *Appl. Phys. Lett.*, vol. 87, no. 22, p. 221105, 2005.
[36] L. Virot, D. Benedikovic, B. Szelag, C. Alonso-Ramos, B. Karakus, J.-M. Hartmann, X. L. Roux, P. Crozat, E. Cassan, D. Marris-Morini, C. Baudot, F. Boeuf, J.-M. Fédéli, C. Kopp, and L. Vivien, "Integrated waveguide PIN photodiodes exploiting lateral Si/Ge/Si heterojunction," *Opt. Express*, vol. 25, no. 16, pp. 19487–19496, 2017.
[37] Z. Zhang, G. I. Ng, T. Hu, H. Qiu, X. Guo, W. Wang, M. S. Rouifed, C. Liu, J. Sia, J. Zhou, C. G. Littlejohns, M. Nedeljkovic, G. T. Reed, and H. Wang, "Experimental Demonstration of Thermally Tunable Fano and EIT Resonances in Coupled Resonant System on SOI Platform," *IEEE Photonics J.*, vol. 10, no. 3, p. 6601108, 2018.
[38] J. X. B. Sia, W. Wang, X. Guo, J. Zhou, Z. Zhang, M. S. Rouifed, X. Li, Z. L. Qiao, C. Y. Liu, C. Littlejohns, G. T. Reed, and H. Wang, "Mid-Infrared, Ultra-Broadband, Low-Loss, Compact Arbitrary Power Splitter Based on Adiabatic Mode Evolution," *IEEE Photonics J.*, vol. 11, no. 2, p. 6601111, 2019.
[39] L. Vivien, A. Polzer, D. Marris-Morini, J. Osmond, J. M. Hartmann, P. Crozat, E. Cassan, C. Kopp, H. Zimmermann, and J. M. Fédél, "Zero-bias 40 Gbit/s germanium waveguide photodetector on silicon," *Opt. Express*, vol. 20, no. 2, pp. 1096-1101, 2012.
[40] W. Jin, D. D. John, J. F. Bauters, T. Bosch, B. J. Thubeault, and J. E. Bowers, "Deuterated silicon dioxide for heterogeneous integration of ultra-low-loss waveguides," *Opt. Lett.*, vol. 45, no. 12, pp. 3340-3343, 2020.
[41] O. Boyraz, and B. Jalali, "Demonstration of a silicon Raman laser," *Opt. Express*, vol. 12, no. 21, pp. 5269–5273, 2004.
[42] H. Rong, A. Liu, R. Jones, O. Cohen, D. Hak, R. Nicolaescu, A. Fang, and M. Paniccia, "An all-silicon Raman laser," *Nature*, vol. 433, no. 7023, pp. 292–294, 2005.
[43] H. Rong, R. Jones, A. Liu, O. Cohen, D. Hak, A. Fang, and M. Paniccia, "A continuous-wave Raman silicon laser," *Nature*, vol. 433, no. 7027, pp. 725–728, 2005.
[44] H. Rong, S. Xu, Y.-H. Kuo, V. Sih, O. Cohen, O. Raday, and M. Paniccia, "Low-threshold continuous-wave Raman silicon laser," *Nat. Photonics*, vol. 1, no. 4, pp. 232–237, 2007.
[45] R. E. Camacho-Aguilera, Y. Cai, N. Patel, J. T. Bessette, M. Romagnoli, L. C. Kimerling, and J. Michel, "An electrically pumped germanium laser," *Opt. Express*, vol. 20, no. 10, pp. 11316–11320, 2012.
[46] T. Komljenovic, M. Davenport, J. Hulme, A. Y. Liu, C. T. Santis, A. Spott, S. Srinivasan, E. J. Stanton, C. Zhang, and J. E. Bowers, "Heterogenous Silicon Photonic Integrated Circuits," *J. Lightwave Technol.*, vol. 34, no. 1, pp. 20-35, 2016.

[47] D. Huang, M. A. Tran, J. Guo, J. Peters, T. Komljenovic, A. Malik, P. A. Morton, and J. E. Bowers, "High-power sub-kHz lasers fully integrated on silicon," *Optica*, vol. 6, no. 6, pp. 745-752, 2019.
[48] C. Xiang, P. A. Morton, and J. E. Bowers, "Ultra-narrow linewidth laser based on a semiconductor gain chip and extended Si_3N_4 Bragg grating," *Opt. Lett.*, vol. 44, no. 15, 2019.
[49] J. X. B. Sia, X. Li, W. Wang, Z. Qiao, X. Guo, J. Zhou, C. G. Littlejohns, C. Liu, G. T. Reed, and H. Wang, "Sub-kHz linewidth, hybrid III-V/silicon wavelength-tunable laser diode operating at the application-rich 1647-1690 nm," *Opt. Express*, vol. 28, no. 17, pp. 25215-25224, 2020.
[50] M. A. Tran, D. Huang, and J. E. Bowers, "Tutorial on narrow linewidth tunable semiconductor lasers using Si/III-V heterogenous integration," *APL Photonics*, vol. 4, p. 111101, 2019.
[51] T. Kita, R. Tang, and H. Yamada, "Narrow Spectral Linewidth Silicon Photonic Wavelength Tunable Laser Diode for Digital Coherent Communication System," *IEEE J. Sel. Top. Quantum Electron.*, vol. 22, no. 6, p. 1500612, 2016.
[52] T. Kita, R. Tang, and H. Yamada, "Compact silicon photonic wavelength-tunable laser diode with ultra-wide wavelength tuning range," *Appl. Phys. Lett.*, vol. 106, no. 11, p. 111104, 2015.
[53] N. Fujioka, T. Chu, and M. Ishizaka, "Compact and Low Power Consumption Hybrid Integrated Wavelength Tunable Laser Module Using Silicon Waveguide Resonators," *J. Lightwave Technol.*, vol. 28, no. 21, pp. 3115–3120, 2010.
[54] H. Guan, A. Novack, T. Galfsky, Y. Ma, S. Fathololoumi, A. Horth, T. N. Huynh, J. Roman, R. Shi, M. Caverley, Y. Liu, T. Baehr-Jones, K. Bergman, and M. Hochberg, "Widely-tunable, narrow-linewidth III-V/silicon hybrid external-cavity laser for coherent communication," *Opt. Express*, vol. 26, no. 7, pp. 7920–7933, 2018.
[55] T. Chu, N. Fujioka, and M. Ishizaka, "Compact, lower-power-consumption wavelength tunable laser fabricated with silicon photonic-wire waveguide micro-ring resonators," *Opt. Express*, vol. 17, no. 16, pp. 14063–14068, 2009.
[56] N. Kobayashi, K. Sato, M. Namiwaka, K. Yamamoto, S. Watanabe, T. Kita, H. Yamada, and H. Yamazaki, "Silicon Photonic Hybrid Ring-Filter External Cavity Wavelength Tunable Lasers," *J. Lightwave Technol.*, vol. 33, no. 6, 2015.
[57] R. Wang, A. Malik, I. Šimonytė, A. Vizbaras, K. Vizbaras, and G. Roelkens, "Compact GaSb/silicon-on-insulator 2.0x μm widely tunable external cavity lasers," *Opt. Express*, vol. 24, no. 25, pp. 28977-28986, 2016.
[58] Z. Zhou, B. Yin, and J. Michel, "On-chip light sources for silicon photonics," *Light-Sci. Appl.*, vol. 4, no. 11, p. e358, 2015.
[59] B. Jalali, and S. Fathpour, "Silicon Photonics," *J. Lightwave Technol.*, vol. 24, no. 12, pp. 4600-4615, 2006.
[60] J. X. B. Sia, W. Wang, Z. Qiao, X. Li, X. Guo, J. Zhou, C. G. Littlejohns, Z. Zhang, C. Liu, G. T. Reed, and H. Wang, "Compact silicon photonic hybrid ring external cavity (SHREC)/InGaSb-AlGaAsSb wavelength-tunable laser diode operating from 1881-1947 nm," *Opt. Express*, vol. 28, no. 4, pp. 5134-5146, 2020.
[61] P. Dong, A. Melikyan, and K. Kim, "Commercializing Silicon Microring Resonators: Technical Challenges and Potential Solutions," *Conference on Lasers and Electro-Optics (CLEO)*, 2018.
[62] W. Bogaerts, P. De Heyn, T. Van Varenbergh, K. De Vos, K. Selvaraja, T. Claes, P. Dumon, P. Bienstman, D. Van Thourhout, and R. Baets, "Silicon microring resonators," *Laser Photonics Rev.*, vol. 6, no. 1, pp. 47-73, 2012.
[63] X. Li, H. Wang, Z. Qiao, X. Guo, W. Wang, J. X. B. Sia, G. I. Ng, Y. Zhang, Z. Niu, C. Tong, and C. Liu, "High temperature characteristics of a 2μm InGaSb/AlGaAsSb passively mode-locked quantum well laser," *Appl. Phys. Lett.*, vol. 114, no. 22, p. 221104, 2019.
[64] X. Li, H. Wang, Z. Qiao, Y. Liao, Y. Zhang, Y. Xu, Z. Niu, C. Tong, and C. Liu, "Temperature- and current-dependent spontaneous emission study on 2 μm InGaSb/AlGaAsSb quantum well lasers," *Jpn. J. Appl. Phys.*, vol. 56, p. 050310, 2017.
[65] P. Walsh, *Lasers and Their Applications*, vol. 1, United Kingdom: ED-Tech Press, 2020, ch. 1, pp. 20-24.
[66] S. Kalchmair, R. Blanchard, T. S. Mansuripur, G.-M. D. Naurois, C. Pfluegl, M. F. Witinski, L. Diehl, F. Capasso, and M. Loncar, "High tuning stability of sampled grating quantum cascade lasers," *Opt. Express*, vol. 23, no. 12, pp. 15734–15747, 2015.
[67] G. Busico, N. D. Whitbread, P. J. Williams, D. J. Robbins, A. J. Ward, and D. C. J. Reid, "A widely tunable Digital Supermode DBR laser with high SMSR," *28th European Conference on Optical Communication (ECOC)*, 2002.

Jia Xu Brian Sia was born in Singapore, on January 28, 1991. During his undergraduate studies, he spent one year on exchange at the University of Strathclyde, Glasgow, United Kingdom. He received the B.E degree at Nanyang Technological University, Singapore, where he is currently a Ph.D. candidate under the supervision of Professor Wang Hong while collaborating with Professor Graham T. Reed's group at the University of Southampton, Optoelectronics Research Centre, Southampton, United Kingdom. In 2018, he spent several months at the Tokyo Institute of Technology, Quantum Nanoelectronics Research Core, Tokyo, Japan, supervised by Professor Shigehisa Arai. His research focuses mainly on hybrid III-V/silicon photonic tunable laser diodes operating at the 2 μm and 1.65 μm waveband, active/passive silicon photonics devices, authoring/co-authoring 20 technical papers thus far.

Brian is a member of the Optical Society of America (OSA) and Institute of Electrical and Electronics Engineers (IEEE).

Wanjun Wang received the B. E. degrees in electronic science and technology from Anhui University, Hefei, China, in 2007 and the Ph.D. degree in microelectronics from Zhejiang University, Hangzhou, China, in 2012. From 2012 to 2016, he worked as engineer and senior engineer in 38th Research Institute, China Electronics Technology Group (CETC). From 2016 to 2017, He was a research fellow in Tohoku University, Japan. He is currently a research fellow at Nanyang Technological University, Singapore. His research interests include the design, fabrication, and characterization of silicon photonic devices working at the near- and mid-infrared wavelengths.

Zhongliang Qiao received the Ph.D. degree in optics engineering from the National Key Laboratory on High Power Semiconductor Lasers, Changchun University of Science and Technology, Jilin, China, in 2011. He was a Postdoctoral Research Fellow in Singapore project (2011–2013) and a Research Fellow (2015–present) in the School of Electrical and Electronic Engineering, Nanyang Technological University, Singapore. His current research interests include growth, design, simulation, fabrication, characterization, and analysis of high performance semiconductor light sources, monolithically integrated multi-wavelength semiconductor laser. He has authored and co-authored more than 60 technical papers in these fields so far.

Xiang Li received the B.Sc. and M.Sc. degrees from Harbin Institute of Technology, China. He is currently a Ph.D. student in the School of Electrical and Electronic Engineering, Nanyang Technological University, Singapore, working on quantum well diode lasers and III-V/Si photonic devices. He has published more than 20 high quality peer-reviewed journal and conference papers.

Tina Xin Guo received the M.S. degree of Engineering from Nanyang Technological University, Singapore, in 2001. She is currently working with Silicon Technologies, Centre of Excellence, Nanyang Technological University, Singapore.

Jin Zhou received the B.Sc. degree of engineering from Australian National University, Australia. She is currently a M.Sc. student in School of Electrical and Electronic Engineering, Nanyang Technological University, Singapore, and working on the nanofabrication.

Callum Littlejohns completed his PhD in the field of Silicon Photonics at the Optoelectronics Research Centre, University of Southampton in March 2015, having previously obtained a First-Class Honours degree in Electronic Engineering at the University of Surrey. He is now part of the CORNERSTONE team in the Silicon Photonics Group at the University of Southampton, working on rapid prototyping of silicon photonics devices. He has a track record of excellence, having received multiple awards throughout his academic life, including the Information Overload category winner at the 2015 EPSRC ICT Pioneers Awards. Callum has published a book chapter, over 30 papers in peer-reviewed journals, and over 100 international conference papers, including a prestigious post-deadline paper at the 2014 IEEE Group IV Photonics conference. The work completed during Callum's PhD has been protected by two separate patents, both fully supported by the University of Southampton.

Chongyang Liu (M'07) received the Ph.D. degree in semiconductor photonics from Nanyang Technological University (NTU), Singapore, in 2004. Currently, he is a Principal Investigator / Senior Research Scientist at Temasek Laboratories, NTU. He was a Research Associate in Singapore-MIT Alliance project (2004–2005) and a Postdoctoral Research Fellow (2005–2007) in the School of Electrical and Electronic Engineering, NTU, Singapore. From 2007 to 2009, he was a Senior Research Fellow with the A∗STAR "VIP" program on Nanophotonics and Nanoelectronic Integration at Data Storage Institute, Singapore. From October 2009 to January 2012, he was awarded a Humboldt Fellowship (for experienced researcher) from Alexander von Humboldt Foundation for doing research in Technical University Berlin, Germany. His research interests include design, simulation, fabrication, characterization, and analysis of low-dimensional semiconductor light sources, monolithically integrated high-speed photonic devices as well as micro/nanophotonic and electronic photonic integration. He has authored and coauthored more than 110 technical papers in these fields so far.

Graham Reed is the Professor of Silicon Photonics at the University of Southampton, UK, He is recognised as one of the pioneers who first established the field of Silicon Photonics worldwide, and he has devoted most of his career to the field. He established the Silicon Photonics Research Group in 1989 (Surrey, then Southampton Universities), and the first Silicon Photonics company, Bookham Technology (now Lumentum), founded by his student Dr Andrew Rickman, emerged from the Group, adopting the work of the Group as their core business. Reed has served on and chaired numerous international conference committees, including founding and chairing the Silicon Photonics Symposium at Photonics West, is currently the Chair of the entire OPTO group of conferences at Photonics West (36 conferences), and is currently a member of 5 other international committees. He has authored more than 500 papers on Silicon Photonics, presented more than 140 Plenary/keynote/invited international talks and filed 19 patents. He has published 2 books including the first Silicon Photonics textbook in the world. Recent prizes and awards include election as a Fellow of SPIE (2012), the IET Crompton Medal for Achievement in Energy (2013) a Royal Society Wolfson Merit Award (2014), election as a Fellow of the Royal Academy of Engineering (2017), best Invited Paper at IEEE BICOP (2018), and PIC Awards Individual Contributor (2019) all for contributions to Silicon Photonics.

Hong Wang received the B.Eng. degree from Zhejiang University, China, in 1988, and the M.Eng. and Ph.D degrees from the Nanyang Technological University (NTU), Singapore, in 1998 and 2001, respectively. From 1988 to 1994, he was with the Institute of Semiconductors, Chinese Academy of Sciences. From 1994 to 1995, he was a Royal Research Fellow with British Telecommunications Laboratories, Ipswich, U.K., where he was involved with the development of InP-based heterostructure field-effect transistors (HFETs) using E-beam lithography. Since 1996, he has been with Nanyang Technological University, where he is currently an Associate Professor, and Director of Nanyang NanoFabrication Centre (N2FC). He has authored or coauthored over 260 technical papers. Prof. Wang was a recipient of the 2007 Defence Technology Prize, Ministry of Defence, Singapore. He served as a session chair, and sub-committee member for 2009 and 2010 IEDM.